Analysis of Competition Binding between Soluble and Membrane-Bound Ligands for Cell Surface Receptors

Ping Li, Periasamy Selvaraj,* and Cheng Zhu

George W. Woodruff School of Mechanical Engineering and Department of Biomedical Engineering, Georgia Institute of Technology, Atlanta, Georgia 30332-0363, and *Department of Pathology and Laboratory Medicine, Emory University School of Medicine, Atlanta, Georgia 30322 USA

ABSTRACT Binding of the Fc portion of IgG coated on targets to Fcγ receptors (e.g., CD16) expressed on leukocytes (i.e., 2D binding) is an initiating step for immune responses such as phagocytosis or antibody-dependent cellular cytotoxicity. In vivo, circulating leukocytes are exposed to plasma IgG. The competition from soluble IgG (i.e., 3D binding) may affect the 2D binding. Many cell surface receptors, CD16 included, have soluble counterparts. While their physiological significance is not clear, receptor-based competitive inhibition therapy, in which soluble receptors, ligands, and their analogs are employed to compete with surface-bound receptors and ligands to prevent unwanted adhesion, is widely used to treat various diseases. To provide a quantitative basis for design of these therapeutic approaches, we developed a mathematical model for 2D and 3D competition binding. The model relates cell-surface adhesion (in the presence and absence of dislodging forces) to the concentration of the soluble competitor, the densities of the surface-bound receptors and ligands, as well as the binding affinities of the 2D and 3D interactions. Binding of CD16-expressing cells to an IgG-coated surface in the presence of a soluble competitor (IgG or anti-CD16 antibody) was quantified by a centrifugation assay. The agreement between experiment and theory supports the validity of the model, which could be useful in predicting the efficacy of the competitor.

INTRODUCTION

Cells communicate with the extracellular environment through their surface receptors. Some receptors interact with surface-bound ligands, such as adhesion proteins and extracellular matrix components. Others bind soluble ligands, such as cytokines and growth factors. In addition, many receptors exist in both surface-bound and soluble forms, produced by alternative splicing of the transcripts or by proteolysis of the membrane receptors. For example, CD16, the Fcγ receptor III (FcγRIII) expressed on the surface of various leukocytes, also exists in circulation (Mathiot et al., 1993). P-selectin, an adhesion receptor for leukocytes expressed on activated platelets and endothelial cells, is also present in the plasma of normal subjects and elevated in patients with thrombotic disorders (Dunlop et al., 1992; Katayama et al., 1993; Ushiyama et al., 1993; Chong et al., 1994). The physiological significance of such a coexistence of both forms is not fully understood. In many cases, however, soluble receptors have been suggested to play an integral part in the dynamic interaction between their membrane-bound counterparts and ligands (Heaney and Golde, 1998).

Similarly, many ligands are present in both forms. Antibodies, which are secreted by B cells as soluble molecules, become surface-bound ligands for the Fc receptors upon binding to antigens deposited on a surface. In a recent work, the immunoglobulin G (IgG) in human sera was shown to inhibit partially or completely the binding of a monoclonal antibody (mAb) 3G8 to CD16a on the surface of monocytes and natural killer (NK) cells (Edberg and Kimberly, 1997). Because 3G8 could effectively block CD16/IgG interaction in cell adhesion experiments, a physiological role for plasma IgG in the competitive inhibition of the binding of cell surface CD16 to immobilized IgG was suggested.

Receptor-based competitive inhibition is an appealing therapeutic strategy that holds promise for the treatment of a wide variety of diseases related to the dysfunction of cell adhesion (Crandall et al., 1993; Martin et al., 1993; Jameson and Bevan, 1995; Kalinke et al., 1996). The idea is to use soluble receptors, ligands, or their analogs to competitively inhibit the unwanted adhesion mediated by surface-linked receptors and ligands. For example, immune thrombocytopenic purpura (ITP) is an autoimmune disease that produces autoantibodies against platelets. Adhesion via Fcγ receptors triggers leukocytes to clear the opsonized platelets. For patients who do not respond to conventional therapy, a high dose of intravenous IgG (Wallace et al., 1997) or anti-FcγR monoclonal antibodies (mAbs) (Clarkson et al., 1986), both of which competitively block the leukocyte Fcγ receptors, may be life saving. Other examples include the use of gp120-binding domain mimics to block HIV binding to CD4 receptors on T cells (Capon et al., 1989). Also, arginine-glycine-aspartic acid (RGD)-containing peptides have been used to inhibit the binding of integrin $\alpha_{IIb}\beta_3$ in thrombosis (Kotze et al., 1995) and to block integrin $\alpha_v\beta_3$-mediated adhesion in osteoporosis (Dresner-Pollak and Rosenblatt, 1994; Chorev et al., 1995).

Thus, not only do both surface-bound and soluble receptors and ligands commonly coexist under physiological

Received for publication 9 March 1999 and in final form 1 September 1999.

Address reprint requests to Dr. Cheng Zhu, School of Mechanical Engineering, Georgia Institute of Technology, Atlanta, GA 30332-0363. Tel.: 404-894-3269; Fax: 404-894-2291; E-mail: cheng.zhu@me.gatech.edu.

0006-3495/99/12/3394/13 $2.00

conditions, but soluble molecules also have been widely used in receptor-based competitive inhibition therapy. In this paper, the adhesive interaction between two surface-bound molecules is referred to as two-dimensional (2D) binding. In comparison, binding of a soluble ligand to a cell surface receptor is called three-dimensional (3D) interaction (Piper et al., 1998). Despite its importance, no mathematical model exists in the literature to describe the competition between 2D and 3D bindings. The present paper describes one such model. This model is useful in assessing whether a naturally existing soluble receptor is able to competitively inhibit the binding of its cell-bound counterpart under physiological conditions. Moreover, the model allows for detailed quantitative analysis of the receptor-based competitive inhibition therapy.

The present 2D/3D competition model is an extension of the well-known theory of 3D/3D competition between two soluble ligands (Cheng and Prusoff, 1973). Because we are interested in cell adhesion mediated by a small number of receptor/ligand bonds under the influence of applied forces, the extension includes two aspects. First, the deterministic formulation of reaction kinetics has been replaced by a probabilistic equivalence, i.e., the master equations (McQuarrie, 1963). Thus we are concerned with the probability of having bonds instead of the (average) density of bonds. Second, not only has one of the binding affinities of the two competitors been changed from 3D to 2D, but it also has become a function of force instead of merely a constant. Both aspects are key elements of a recently developed model for 2D receptor/ligand binding in cell adhesion (Piper et al., 1998). The new addition in the present model is the inclusion of a 3D competitor in the binding scheme.

Our theoretical model was tested experimentally, using a centrifugation assay (McClay et al., 1981), and was found to be consistent with the data. While this is similar to our previous work (Piper et al., 1998), the present experiment added a new variable—the soluble competitor. Instead of the E-selectin/carbohydrate ligand system used in our earlier work, the present study employed the CD16/IgG system. CD16 is a 50–80-kDa low-affinity leukocyte receptor for the Fc portion of IgG (FcγRIII) (Hibbs et al., 1989; Scallon et al., 1989; Selvaraj et al., 1989). Binding of CD16 to aggregated IgG triggers a variety of immune responses, including receptor-mediated phagocytosis, antibody-dependent cellular cytotoxicity, and release of inflammatory mediators (Lanier et al., 1989; Letourneur et al., 1991; O'Shea et al., 1991; Nagarajan et al., 1995). Our experiment quantified adhesions of CD16-expressing cells to surface-bound IgG in the presence of either a similar (IgG) or dissimilar (anti-CD16 mAb) competitor in solution. This design was chosen for its physiological relevance, as it represents an in vitro model for ITP and other autoimmune diseases involving leukocyte FcγRs and deposited immune complexes. The similar competitor experiment mimics the treatment of ITP with high doses of intravenous IgG (Wallace et al., 1997) as well as other situations in which soluble molecules compete with their surface-bound counterparts. The dissimilar competitor experiment mimics the treatment of ITP with anti-FcγR mAbs (Clarkson et al., 1986) as well as other situations in which high-affinity analogs or mAbs are employed for receptor-based competitive inhibition therapy.

The formula of Cheng and Prusoff (1973) for 3D/3D competition provides the basis for a method of measuring binding affinity too low to be directly measured by the Scatchard analysis (Scatchard, 1949). Similarly, our 2D/3D competition model can be used to measure affinities of the respective surface-bound and soluble ligands when combined with a quantitative assay for cell adhesion, such as the centrifugation assay (Piper et al., 1998). The efficacy of a soluble competitor is usually measured by a phenomenological index, IC_{50} (i.e., the concentration required to inhibit adhesion by 50%). Such a definition is adapted from the convention of the 3D/3D competition (Cheng and Prusoff, 1973), where IC_{50} is a function of the affinities of the ligand and its competitor as well as concentrations for all reactive species. For the case of 2D/3D competition, IC_{50} also depends on an additional variable, the dislodging force applied to remove the less adherent cells, as one might expect. While the exact mathematical relationship between IC_{50} and these parameters is fairly complex, a useful result derived from the present work is that IC_{50} is approximately equal to the dissociation constant of the 3D competitor when adhesion is sufficiently low. Another simple approximate equation relates the competitor concentration required to inhibit adhesion to a low level (say, <20%) to the receptor and ligand densities, as well as the 2D and 3D affinities. This formula may be used to guide the dosage in competitive inhibition therapy.

THEORETICAL DEVELOPMENT

Governing equations

The reaction in question is

$$R + C \underset{k_{r,3D}}{\overset{k_{f,3D}}{\rightleftharpoons}} B_{3D} \quad \text{outside contact area} \tag{1a}$$

$$2R + L + C \underset{k_{r,2D},\,k_{r,3D}}{\overset{k_{f,2D},\,k_{f,3D}}{\rightleftharpoons}} B_{2D} + B_{3D} \quad \text{inside contact area} \tag{1b}$$

where R, L, C, and B denote, respectively, receptor, ligand, soluble competitor, and bond. The subscript in B indicates whether the bond is 2D (i.e., between two surface-bound molecules) or 3D (i.e., between a surface-linked molecule and a soluble competitor). The forward and reverse rates, k_f and k_r, are also given a 2D or 3D designation. Traditionally, the kinetics of reaction Eq. 1a is described by

$$\frac{d[B_{3D}]}{dt} = k_{f,3D}[R][C] - k_{r,3D}[B_{3D}] \tag{2a}$$

where t is time and the square brackets denote concentrations. Such a deterministic kinetic equation assumes a large

system of reactive molecules. This is usually true outside the contact area between the cell and the substrate surface. Inside the contact area A_c, however, the system is small and the stochastic characteristics of binding become apparent (Piper et al., 1998; Chesla et al., 1998; Long et al., 1999). The master equations are required to describe the probabilistic kinetics of the reaction in Eq. 1b:

$$\begin{aligned}\frac{dp_n^m}{dt} &= k_{f,2D}^{(n)} m_l[A_c m_r - m - (n-1)]p_{n-1}^m + k_{r,2D}^{(n+1)}(n+1)p_{n+1}^m \\ &+ k_{f,3D} c[A_c m_r - (m-1) - n]p_n^{m-1} \\ &+ k_{r,3D}(m+1)p_n^{m+1} \\ &- [k_{f,2D}^{(n+1)} m_l(A_c m_r - m - n) + k_{r,2D}^{(n)} n \\ &+ k_{f,3D} c(A_c m_r - m - n) + k_{r,3D} m]p_n^m \end{aligned} \quad (2b)$$

where p_n^m is the probability of having m 3D bonds and n 2D bonds within A_c. m_r and m_l are the respective total densities of receptors and ligands. c is the concentration of the soluble competitor. In addition to the Markovian process and sequential binding assumptions that underlie the master equations (McQuarrie, 1963), it is further assumed that m_l and c are much greater than the respective density and concentration of the 2D and 3D bonds. These are valid assumptions in the centrifugation experiment (Piper et al., 1998).

In contrast to the constant 3D rates, the 2D rates depend on the force applied to the cell and the number of 2D bonds sharing that force, as indicated by the superscript n. For the present work that only deals with the steady state, it is sufficient to express such a dependency in a constitutive equation for the 2D affinity:

$$K_{a,2D}\left(\frac{f}{n}\right) \triangleq \frac{k_{f,2D}^{(n)}}{k_{r,2D}^{(n)}} = K_{a,2D}^0 \exp\left(-\frac{af}{nk_BT}\right) \quad (3)$$

where a is a bond parameter, k_B is the Boltzmann constant, and T is the absolute temperature. Among the several models proposed for the dependence of 2D affinity on dislodging force, Eq. 3 was chosen for its simplicity. It has been shown to be an appropriate model for the E-selectin binding data generated with the centrifugation assay (Piper et al., 1998). It will be demonstrated later that Eq. 3 also describes the CD16/IgG binding data well.

Relation to existing models

Reduction of Eq. 2b to its deterministic counterpart can be done by multiplying both sides of Eq. 2b by m (or n) and summing over both m and n to obtain two equations for the average numbers of 3D ($\langle m\rangle$) and 2D ($\langle n\rangle$) bonds:

$$\frac{d\langle m\rangle}{dt} = k_{f,3D} c(A_c m_r - \langle m\rangle - \langle n\rangle) - k_{r,3D}\langle m\rangle \quad (4a)$$

$$\begin{aligned}\frac{d\langle n\rangle}{dt} &= \langle k_{f,2D}^{(n+1)}\rangle m_l(A_c m_r - \langle m\rangle - \langle n\rangle) - \langle k_{r,2D}^{(n)}\rangle\langle n\rangle \\ &- m_l(\langle k_{f,2D}^{(n+1)} m\rangle - \langle k_{f,2D}^{(n+1)}\rangle\langle m\rangle) - m_l(\langle k_{f,2D}^{(n+1)} n\rangle \\ &- \langle k_{f,2D}^{(n+1)}\rangle\langle n\rangle) - (\langle k_{r,2D}^{(n)} n\rangle - \langle k_{r,2D}^{(n)}\rangle\langle n\rangle) \end{aligned} \quad (4b)$$

where $\langle\ \rangle$ denotes averaging. Relating the average numbers of bonds to their densities, Eq. 4 can be recognized as the deterministic kinetic equations for reaction Eq. 1b. When both sides are divided by a volume to convert numbers of molecules to their concentrations, Eq. 4a becomes identical to Eq. 2a. The three terms in the parentheses on the second line of Eq. 4b are cross-correlation functions resulting from the dependence of the 2D kinetic rates on n. They are measures of fluctuations and as such their contributions to Eq. 4b diminish as the system becomes large and statistically stable. The steady-state and large system limit of Eq. 4 (obtainable by setting the left-hand side to zero and neglecting the cross-correlation terms) is equivalent to the equations from which the 3D/3D competition binding theory is derived (Cheng and Prusoff, 1973).

Needless to say, it is the 2D not 3D bonds that mediate the physical linkage of cell adhesion. The marginal probability distribution of the 2D bonds is defined by $p_n = \Sigma_m p_n^m$. Summing Eq. 2b over m, one obtains

$$\begin{aligned}\frac{dp_n}{dt} &= k_{f,2D}^{(n)} m_l[A_c m_r - (n-1)]p_{n-1} + k_{r,2D}^{(n+1)}(n+1)p_{n+1} \\ &- [k_{f,2D}^{(n+1)} m_l(A_c m_r - n) + k_{r,2D}^{(n)} n]p_n \\ &+ m_l \sum_m m(k_{f,2D}^{(n+1)} p_n^m - k_{f,2D}^{(n)} p_{n-1}^m) \end{aligned} \quad (5)$$

This is the binomial type of the masters equations discussed by Piper et al. (1998), except for the addition of the last summation term on the right-hand side.

Approximate solutions

In the absence of active spreading, the number of 2D bonds is typically very small, as their formation is limited by the cell surface roughness (Piper et al., 1998; Chesla et al., 1998; Williams, 1998). In contrast, soluble competitors can access all unoccupied cell surface receptors, even if they are hidden in the membrane folds (Williams, 1998). As such, the number of 3D bonds is much larger, even at low competitor concentrations. This allows us to neglect the fluctuations in the 3D bonds and to approximate the summation terms in Eq. 5 by

$$\sum_m m p_n^m \approx \langle m\rangle p_n \approx p_n A_c m_r/(1 + K_{d,3D}/c) \quad (6)$$

The first approximate expression in Eq. 6 would not be exact unless the two ligands were independent (C. Zhu and T. E. Williams, manuscript submitted for publication), which is not the case here because the surface and soluble ligands are in competition for the same receptor. The second approximate expression in Eq. 6 follows from Eq. 4a (the

steady-state version) when $\langle m \rangle \gg \langle n \rangle$, which is clearly the case here. Substituting Eq. 6 into Eq. 5 recovers the binomial type of the masters equations discussed by Piper et al. (1998), except that the receptor number in the contact area, $A_c m_r$, is now scaled by a factor $(1 + cK_{a,3D})$. Its steady-state solution applicable to the centrifugation experiment is (Piper et al., 1998)

$$p_n = p_0 \binom{A_c m_r/(1 + cK_{a,3D})}{n} \prod_{i=1}^{n} m_l K_{a,2D} \left(\frac{f}{i}\right) \quad n > 0 \tag{7a}$$

where

$$p_0 = \left[1 + \sum_{n=1}^{A_c m_r/(1+cK_{a,3D})} \binom{A_c m_r/(1 + cK_{a,3D})}{n} \prod_{i=1}^{n} m_l K_{a,2D} \left(\frac{f}{i}\right)\right]^{-1} \tag{7b}$$

The probability of adhesion is that of having at least one bond, i.e., $P_a = 1 - p_0$.

The validity of the above approximate solutions is tested in Fig. 1, where the ratio of P_a given by Eq. 7b to that of the exact solution to the full master equations (Eq. 2b) is plotted against $A_c m_r/(1 + cK_{a,3D})$ for various $cK_{a,3D}$ (Fig. 1 *A*) and $m_l K^0_{a,2D}$ (Fig. 1 *B*). These parameters represent the respective propensities of forming 3D and 2D bonds. It is evident that when $A_c m_r/(1 + cK_{a,3D})$ approaches 1, the approximation breaks down, as revealed by the significant deviation of the P_a ratio from unity. However, as $A_c m_r/(1 + cK_{a,3D})$ increases beyond 10, i.e., the average number of 3D bonds is large relative to $cK_{a,3D}$, the P_a ratio quickly approaches unity, indicating that Eq. 7 is a good approximation to the exact solution to Eq. 2b in these parameter regimes, which correspond to the conditions of our experiment.

Following Piper et al. (1998), an approximate solution can be derived for the case of rare adhesion, $P_a \ll 1$:

$$P_a \approx A_c m_r m_l K_{a,2D}(f)/(1 + cK_{a,3D}) \tag{8}$$

Setting $c = 0$ reduces Eqs. 7 and 8 to the corresponding equations discussed by Piper et al. (1998), as required.

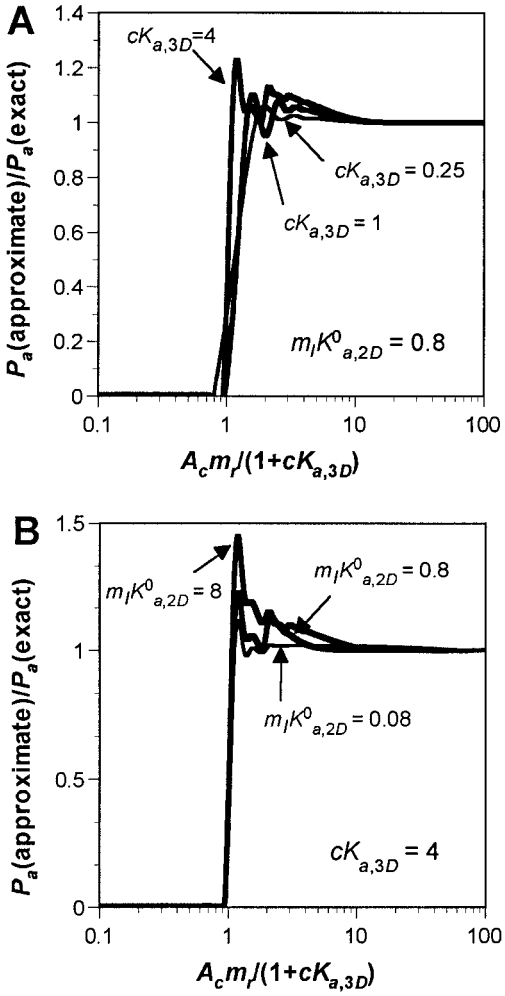

FIGURE 1 Comparison between exact and approximate solutions to the master equations. The P_a $(= 1 - p_0)$ ratio of the approximate analytical solution, Eq. 7b, to the numerical solution to the full master equations, Eq. 2b, is plotted against the available receptor number in contact area $A_c m_r/(1 + cK_{a,3D})$ $(\sim\langle m \rangle/cK_{a,3D})$ for various $cK_{a,3D}$ (*A*) and $m_l K^0_{a,2D}$ (*B*) values as indicated. Note that the experimental conditions in the present work satisfy $A_c m_r/(1 + cK_{a,3D}) \gg 10$, which is within the parameter range that validates the approximation.

Relating IC_{50} to affinity

By definition, IC_x is the concentration of the soluble competitor required to achieve x% of inhibition. For the case of nearly complete inhibition, Eq. 8 is applicable:

$$IC_x \approx \left[\frac{A_c m_r m_l K_{a,2D}(f)}{(1 - x\%)P_{a,0}} - 1\right] K_{d,3D} \tag{9}$$

where $P_{a,0}$ is the adherent fraction in the absence of a soluble competitor. This is similar to the Cheng and Prusoff formula for measuring the dissociation constant, $K_{d,3D}$, of a competitor for its receptor, using a ligand of known affinity. The Cheng and Prusoff equation was derived for 3D/3D competition, whereas Eq. 9 applies to 2D/3D competition. Because IC_x is proportional to $K_{d,3D}$, the higher the competitor's affinity, the lower the concentration required to achieve the same level of inhibition. Thus Eq. 9 offers a design tool for receptor-based competitive inhibition therapy, which may be used to guide the dosage of inhibitor administration.

$P_{a,0} \approx A_c m_r m_l K_{a,2D}(f)$ when $P_{a,0}$ itself is small compared to unity, which results in further simplification of Eq. 9:

$$K_{d,3D} \approx \frac{1 - x\%}{x\%} IC_x \tag{10a}$$

In particular, when $x = 50$,

$$K_{d,3D} \approx IC_{50} \tag{10b}$$

Thus, when adhesion is infrequent, the 3D equilibrium dissociation constant can be approximated by the IC_{50}. These results are interesting and may be useful in designing simple experiment to estimate the $K_{d,3D}$ (see Results).

MATERIALS AND METHODS

Cells and antibodies

Our CD16a-expressing Chinese hamster ovary (CHO) cell transfectants have previously been described (S. E. Chesla, P. Li, S. Nagarajan, P. Selvaraj, and C. Zhu, manuscripts submitted for publication). The anti-CD16 mAb CLBFcgran-1 (murine IgG2a) and irrelevant control mAb X63 (murine IgG1) were purified in house from hybridomas as previously described (Selvaraj et al., 1988). The cleaving of CLBFcgran-1 into Fab fragment was done by Lampire (Pipersville, PA). The fluorescein isothiocyanate (FITC)-conjugated goat anti-mouse polyclonal antibody used in flow cytometry was purchased from Sigma Chemical Company (St. Louis, MO). Two types of rabbit (Rb) IgG were also purchased from Sigma. One was a specific polyclonal antibody against bovine serum albumin (BSA) (in IgG fraction), which was used as a surface-bound ligand. The other was nonspecific RbIgG that did not react with BSA and would not be absorbed onto a BSA-coated plastic surface. This was used as a soluble competitor.

Receptor density determination

Quantitative indirect fluorescent immunoassay (QIFI) (Serke et al., 1998; Bikoue et al., 1996) was used to quantify the expression of CD16a on CHO cell transfectants, as previously described (Chesla et al., 1998). We found that receptor site density measured by QIFI correlated well with radioimmunoassay (RIA) using ^{125}I-labeled proteins (Chesla et al., 1998). Briefly, CD16a-expressing CHO cells stained with primary mAbs CLBFcgran-1 (anti-CD16) or X63 (negative control) and FITC-conjugated anti-mouse secondary antibody were analyzed by flow cytometry. A calibration curve between the mean fluorescence intensity and the number of FITC molecules was generated using standard beads. The number of CD16a on the CHO cell surface was calculated based on the number of FITC molecules per cell and per anti-mouse goat antibody (provided by the manufacturer).

Labeling anti-BSA RbIgG with FITC

Anti-BSA RbIgG was dialyzed with FITC labeling buffer for 2 days with three buffer changes. Ten microliters of 10 mg/ml FITC (Sigma) in dimethyl sulfoxide was added to 1 ml of 1 mg/ml RbIgG. The mixture was incubated for 2 h at room temperature. The FITC-labeled RbIgG was dialyzed with phosphate-buffered saline (PBS) for 2 days with three buffer changes.

Coating of RbIgG and determination of their surface density

Previously, we quantified the surface density of coated molecules by RIA (Piper et al., 1998). In the present work the site density of immobilized anti-BSA RbIgG was determined fluoremetrically. Ninety-six-well microtiter plates (Corning, Cambridge, MA) were coated with 1% IgG-free BSA (Sigma) in PBS/EDTA at 4°C overnight. After two washes with PBS/EDTA, variable concentrations of unlabeled (for centrifugation experiment) or FITC-labeled (for site density determination) anti-BSA RbIgG in PBS were added to the wells (50 μl per well) and incubated for 30 min at 4°C. In some control centrifugation experiments nonspecific RbIgG not reactive to BSA was used instead of anti-BSA RbIgG. The wells were washed with PBS/EDTA twice before being used in the centrifugation experiment or being read in a fluorescence plate reader (Biorad, Hercules, CA) for site density determination. As shown in Fig. 2 *A*, the measured fluorescence intensity appears to be a linear function of the mass of FITC-labeled RbIgG in the range tested. Using this as calibration, we determined the relationship between the site density of RbIgG immobilized on 96-well plates and the RbIgG solution concentration used to coat the surface, as showed in Fig. 2 *B*. The linear relationship seen in Fig. 2 *B* indicates that the concentration of anti-BSA RbIgG used was well below that required to saturate the BSA sites on the wells coated with 1% BSA.

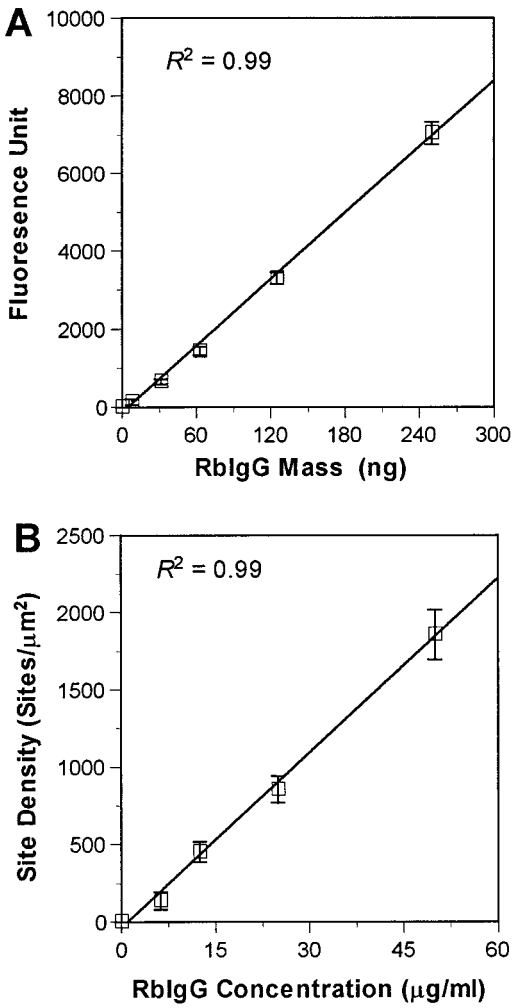

FIGURE 2 Determination of RbIgG coating density. (*A*) FITC-conjugated anti-BSA RbIgG of a known amount (0, 15.6, 31.2, 62.5, 125, and 250 ng) was added to wells of a 96-well plate. The wells were read with a fluorescence plate reader. The fluorescence intensity of the wells without FITC-RbIgG was used as the background and subtracted from the reading of wells with FITC-RbIgG. Data (*points*) were presented as mean ± standard deviation of quadruplicate wells. A straight line was fit to the data. (*B*) FITC-labeled anti-BSA RbIgG of known concentrations (0, 3.1, 6.2, 12.5, 25, and 50 μg/ml) was immobilized on BSA-coated wells of a 96-well plate as described in the text. After the background was subtracted (fluorescence reading of the wells without FITC-RbIgG), the fluorescence reading was converted to site density, using the relationship established in *A*. The line is a linear fit to the data (*points*, mean ± standard deviation of quadruplicate wells).

Gel filtration

Aggregated IgG is a multivalent ligand and binds to CD16 with high avidity. Therefore, the presence of even a small fraction of aggregated IgG

may lead to erroneous result in assays intended for monomeric IgG. In order to remove large-sized aggregated IgG, before each centrifugation experiment 150 mg of RbIgG in 5 ml PBS/EDTA was spun in a microcentrifuge at high speed at 4°C. The monomeric RbIgG was further separated from oligomers by size exclusion chromatography. Briefly, RbIgG in 5 ml PBS/EDTA was passed through a Sephadex G-200 (Pharmacia, Piscataway, NJ) column (500 ml in bed volume, 2.5 cm in diameter). The flow rate was set to be 0.25 ml/min. The flow through was collected by a fraction collector (Biorad) with 5 ml in each fraction. The optical density of each fraction was measured in a spectrometer at 280 nm. Fractions of monomeric or aggregated IgG were concentrated in protein concentrators (Millipore, Bedford, MA), the concentrations of which were determined with a protein estimation kit (Biorad). When the concentrated monomeric RbIgG was passed through the gel filtration column again only a single peak was seen, indicating that the concentration procedure did not produce reaggregation. The centrifugation experiments were always done immediately after the gel filtration and concentration.

Fluorescent labeling of CHO cells

CHO cells were detached by and washed twice with PBS/EDTA. They were resuspended in PBS at 5×10^6 cells/ml. Ten mg/ml of calcein AM (Molecular Probes, Eugene, OR) was added to the cell suspension in the ratio of 1 μl to 1 ml. The cells were incubated at room temperature for 30 min. The labeled cells were washed twice with binding buffer (0.4% OVA (Sigma) in PBS/EDTA). For each batch of labeled cells, a calibration curve was generated to relate the fluorescence intensity and the number of cells present. As can be seen in Fig. 3, the fluorescent intensity of the wells appears as a linear function of the number of labeled CHO cells, providing a simple conversion between the two. The present fluorometric method has several advantages over our previous radiometric technique using ^{51}Cr-labeling (Piper et al., 1998). The 96-well plate can be read directly by a fluorescence plate reader without transferring the individual wells to the γ counter.

Centrifugation experiment

One hundred fifty microliters of fluorescently labeled CD16a-expressing CHO cells at a concentration of 2×10^5 cells/ml in binding buffer with varying concentrations of soluble competitor (RbIgG or Fab fragment of CLBFcgran-1) was added to each anti-BSA RbIgG-coated well and incubated for 45 min at 4°C. The wells were filled up with corresponding concentrations of competitor in binding buffer, incubated for another 45 min at 4°C, then sealed with plate sealers and spun in a centrifuge at a desired speed for 3 min. The plates were inverted in cold PBS/EDTA to remove detached cells and read by a fluorescent plate reader. The fraction of adherent cells was calculated in a fashion similar to that of the calculation of the ligand site density, using standards to remove nonspecific contribution and to convert fluorescence intensity into cell numbers.

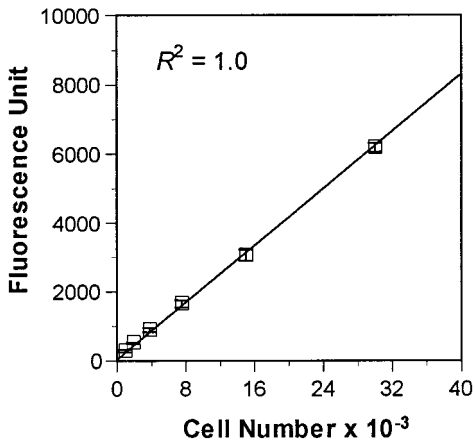

FIGURE 3 Fluorometric determination of adherent cells. CD16a-expressing CHO cells were labeled with calcein AM. Suspensions containing a known number of cells (0, 938, 1,875, 3,750, 7,500, 15,000, and 30,000) were added to the wells of a 96-well plate via serial dilution. The plate was read with a fluorescence plate reader. The fluorescence reading of the wells without cells was used as the background and subtracted from the reading of wells with cells. Data (*points*) were presented as mean ± standard deviation of quadruplicate wells. A straight line was fit to the data.

Size and density measurements of CHO cells

The centrifugal force (f, in pN) was calculated from the spinning speed (ω, in rad/s), the distance from the cell and the axis of rotation (l, in m), and the volume (V, in μm^3) and density (ρ_c, in g/cm^3) of the CHO cells according to $f = \omega^2 l(\rho_c - \rho_m)$, where ρ_m is the medium density. Cell size was directly measured microscopically, which followed a broad log normal distribution as previously noted for other cells (Piper et al., 1998). The mean and standard deviation of the cell volume were 1351 and 617 μm^3, respectively. The density of the CHO cells was measured by centrifugation through a continuous density gradient with calibration beads of known densities (Zhu et al., 1999). The result was $\rho_c = 1.050$ g/cm^3.

Numerical solution of master equations

Equations 2b and 3 were solved at steady state, using an iterative algorithm. Briefly, upon assuming an initial set of $p_n^m(t_i)$ the p_n^m values at the next time point t_{i+1} were calculated from $(p_n^m(t_{i+1}) - p_n^m(t_i))/(t_{i+1} - t_i) = \mathrm{RHS}(t_i)$, where RHS is the right-hand side of Eq. 2b. The iteration continued with increasing i values until $\max_n|p_n^m(t_{i+1}) - p_n^m(t_i)| \le \epsilon$, where ϵ is the assigned convergence criterion ($<10^{-5}$). $p_n^m(t_{i+1})$ was the solution at equilibrium.

RESULTS

Confirmation of binding specificity

Fig. 4 shows that CD16a-expressing CHO cells bound well to wells incubated consecutively with IgG-free BSA and rabbit anti-BSA antibody. In contrast, the same CHO cells did not bind to BSA-treated wells with or without the second-step incubation with irrelevant RbIgG, indicating the requirement of surface-bound ligand. Similarly, untransfected CHO cells or CHO cells transfected to express an irrelevant receptor, B7, did not bind to wells incubated consecutively with BSA and anti-BSA RbIgG, indicating the requirement for the cell surface receptor. Therefore, it was confirmed that the adhesion assayed here was indeed mediated by the specific binding of cell surface CD16a to anti-BSA RbIgG coated on the wells. The binding specificity was further demonstrated in the competition experiment, where adhesion was inhibited progressively by soluble RbIgG and Fab fragment of CLBFcgran-1 (Figs. 6 and 9).

Testing the steady-state assumption

The temporal resolution of the centrifugation assay is on the order of a minute, which is longer than the transient time scale (seconds) of the CD16a-IgG-mediated cell adhesion as characterized by the reciprocal kinetic rate constants,

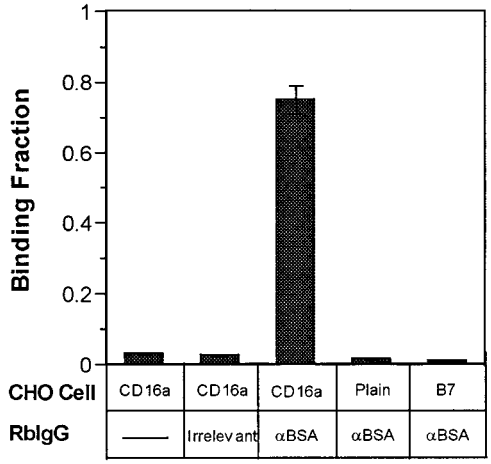

FIGURE 4 Demonstration of binding specificity. The wells of a 96-well plate coated with IgG-free BSA were incubated with 25 μg/ml of anti-BSA RbIgG or irrelevant RbIgG that did not react with BSA or plain PBS (—). The adhesion to these wells of fluorescently labeled untransfected CHO cells (plain) or CHO cells transfected to express CD16a or B7 was assayed in a centrifugation experiment (300 rpm) as described in the text. It is evident that significant binding occurred only between CD16a-expressing CHO cells and BSA-coated wells treated with anti-BSA RbIgG.

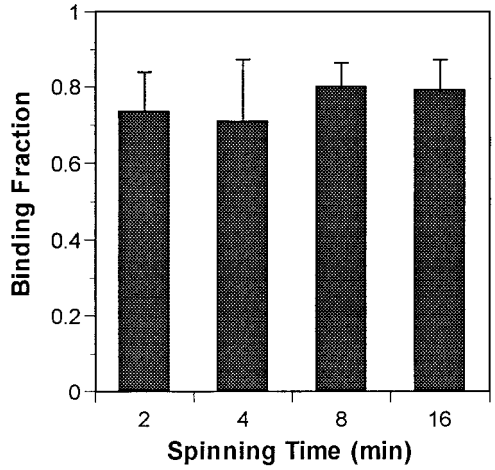

FIGURE 5 Lack of effect of spinning duration on cell detachment. Binding of CD16a-expressing CHO cells to wells coated with 450 sites/μm^2 anti-BSA RbIgG in the presence of 53 μg/ml of soluble RbIgG (nonreactive to BSA) was assayed by centrifugation at 300 rpm for different spinning times (2, 4, 8, and 16 min). Data are presented as mean + standard deviation of quadruplicate wells.

$1/(m_r m_l A_c k_f)$ and $1/k_r$ (Chesla et al., 1998; Chesla et al., manuscript submitted for publication). For this reason, the steady-state solution of our model, Eq. 7, was used to analyze the centrifugation data. To ensure the achievement of a steady state in our experiments, the cells were incubated with the ligand-coated surface for a total of 90 min during the attachment phase. During the detachment phase the steady-state assumption was tested by spinning the cells over varying periods of time. The lack of dependence of the adherent fraction on the duration of force application up to 16 min is clearly evident from Fig. 5. These data suggest that the steady state had been reached before the shortest time point (2 min) tested, as prolonged spinning at the same speed did not detach any more cells.

Inhibition of CD16a-expressing CHO cell adhesion to RbIgG-coated surface by similar competitor

In one set of centrifugation experiments, soluble RbIgG was allowed to compete with surface-bound RbIgG for binding of cell surface CD16a. This was designed to address the question of whether the serum IgG would prevent binding of leukocyte FcγRs to IgG immobilized on surfaces of target cells or blood vessel walls. These data should also be relevant to receptor-based competitive inhibition therapy, in which a competitor similar to the surface-bound molecule is used.

To minimize interexperimental variations, we used the same batch of cells in side-by-side experiments and simultaneously measured their adhesions to wells coated with four different anti-BSA RbIgG densities, in the presence of six different soluble RbIgG (nonreactive to BSA) concentrations, and under four different centrifugal forces. Representative data are exemplified in Fig. 6. It is evident that, for a given ligand coating density and centrifugal force, the adhesion fraction decreased with the increasing soluble competitor concentration. Also, the adhesion fraction increased with increasing surface ligand coating density for fixed competitor concentration and centrifugal force. Finally, for any competitor concentration and ligand coating density, the adhesion fraction decreased with the increasing centrifugal force. These qualitative trends appear reasonable, as they follow an expected pattern.

Comparison of theory to experiment

To test the validity of the model, the solution to Eqs. 2b and 3 (curves) was fit to the experimental data (points) in Fig. 6. It should be emphasized that we fitted the prediction to the entire set of data of a total of 16 curves with six points for each curve, not just an individual curve. As can be seen from Fig. 6, the agreement between the theory and experiment is surprisingly good, considering the complexity of the data (multivariables, wide ranges, and large number of points) and the limited number of free fitting parameters. The agreement between theory and experiment thus supports the validity of our model. The three fitting parameters are the 3D and 2D affinities, $K_{a,3D}$ and $A_c K^0_{a,2D}$, and the bond parameter, a. The best-fit values of these are listed in Table 1.

Dependence of IC_{50} on ligand density and centrifugal force

Each inhibition curve in Fig. 6 has its own IC_{50}, the concentration of the soluble competitor required to achieve

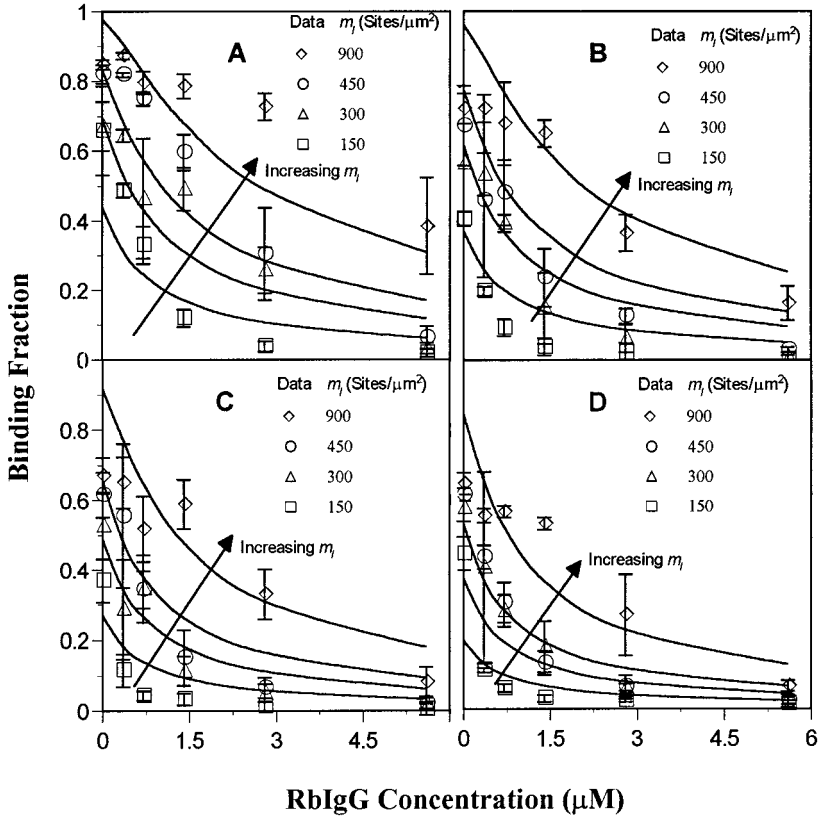

FIGURE 6 Centrifugation experiment with similar competitor. Binding of CHO cells expressing 860 sites/μm^2 of CD16a to variable densities (indicated) of surface-bound anti-BSA RbIgG in the presence of different concentrations (0, 53, 105, 210, 420, and 840 μg/ml) of soluble RbIgG (nonreactive to BSA) was assayed by centrifugation at 300 (*A*), 450 (*B*), 630 (*C*), and 760 (*D*) rpm. Data (*points*) are presented as mean ± standard deviation of quadruplicate wells. The curves are a single least χ^2 fit to all of the data based on Eqs. 2b and 3. The experiment was repeated three times, and the results shown are representative.

50% of inhibition. While this phenomenological index is commonly used to measure the efficacy of a soluble competitor, it should be emphasized that IC_{50} depends on m_l, the RbIgG coating density, and f, the applied centrifugal force. This dependence was measured from the experimental data in Fig. 6 and compared to the model predictions, as shown in Fig. 7. As expected, the higher the adhesion (as a result of higher ligand density and/or lower the centrifugal force), the higher the competitor concentration required to achieve the same level of inhibition, and thereby the higher the IC_{50}. Only when the adhesion fractions become small do all IC_{50} curves approach a constant. Our model predicts that this constant is $K_{d,3D}$, the equilibrium dissociation constant of the soluble competitor for the cell surface receptor. It is evident from Fig. 7 that this prediction is supported by the data. Thus $K_{d,3D}$ can be estimated from IC_{50}, using a simple adhesion assay, provided that the initial binding in the absence of the competitor is sufficiently low.

TABLE 1 Summary data (best-fit value ± standard deviation) for CD16a binding affinity

Soluble competitor	$K_{a,3D}$ (M^{-1})	$A_c K^0_{a,2D}$ (μm^4)	a (nm)
RbIgG	$(2.0 \pm 0.085) \times 10^6$	$(8.0 \pm 0.19) \times 10^{-6}$	0.1 ± 0.02
CLBFcgran-1	$(9.1 \pm 0.22) \times 10^8$	$(7.5 \pm 0.18) \times 10^{-6}$	0.1*

Three-dimensional affinities are for soluble competitors (RbIgG and Fab fragment of CLBFcgran-1). Two-dimensional affinities are for surface-bound RbIgG but measured from experiments using difference soluble competitors.

* Not a fitting parameter but fixed as model input.

Direct measurement of $A_c K_{a,2D}(f)$

The reduced adhesion when a higher centrifugal speed was applied (Fig. 6) suggests a decrease in the 2D affinity with

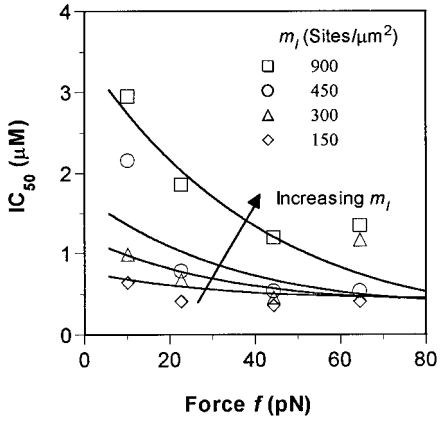

FIGURE 7 Dependence of IC_{50} on ligand density and centrifugal force. IC_{50} corresponding to different m_l was measured from the data in Fig. 6 and plotted against f (*points*). The curves were theoretical predictions based on Eqs. 2b and 3 and parameter values $A_c K^0_{a,2D} = 8.0 \times 10^{-6}$ μm^4 and a = 0.1 nm. These curves asymptotically approach a horizontal line that intercepts the y axis at 0.5 μM, which is equal to $K_{d,3D}$ (cf. Table 1).

increasing dislodging force, as modeled by Eq. 3. In addition to fitting Eqs. 2b and 3 to all data in Fig. 6 to evaluate the model parameters and then using Eq. 3 to predict $A_cK_{a,2D}(f)$, the dependence of the 2D affinity on force can also be directly measured from the low adhesion data points ($P_a < 0.2$) in Fig. 6. For each centrifugal force and ligand density, $P_a(1 + cK_{a,3D})/m_lm_r$ values were calculated and averaged over all competitor concentrations to give rise to an estimate for $A_cK_{a,2D}$ (see Eq. 8). This was plotted against force in Fig. 8 for each ligand density. The lack of dependence of the $A_cK_{a,2D}$ versus f curve on m_l supports the validity of Eq. 8. Using Eq. 3 and parameters listed in Table 1, the force dependence of the 2D affinity was plotted in Fig. 8. It is evident that the theoretical curve compares quite well with the directly measured $A_cK_{a,2D}(f)$ data, providing further support for our model.

Inhibition of CD16a-expressing CHO cell adhesion to a RbIgG-coated surface by dissimilar competitor

In another set of centrifugation experiments, the soluble competitor was changed to CLBFcgran-1, which was different from the surface-bound ligand. This was designed to determine the concentration at which a mAb directed against CD16 would be effective in blocking unwanted adhesion mediated by the CD16/IgG interaction. These data should also be relevant to receptor-based competitive inhibition therapy, in which antibodies or receptor or ligand analogs are used as competitors.

The fractions of CD16a-expressing CHO cells adherent to wells coated with four different anti-BSA RbIgG densities were measured in the presence of six different soluble CLBFcgran-1 concentrations. Fab fragment was used instead of the whole antibody to ensure 1:1 stoichiometry and to avoid the potential interaction of the Fc portion of the murine IgG with CD16a. Typical results are shown in Fig. 9. The pattern of inhibition of CHO cell adhesion by CLBFcgran-1 is similar to that by soluble RbIgG, except that a much lower concentration of CLBFcgran-1 is needed for the same level of inhibition. This is expected, as CLBFcgran-1 has a much higher affinity for CD16a than RbIgG. The curves are the least χ^2 fitting of the solution to Eqs. 2b and 3 to the experimental data. Because centrifugal force was not varied in this experiment, it was not possible to determine the bond parameter from the data. Instead, the same a value (=0.1 nm) as estimated from the data in Fig. 6 was used as an input to the model, leaving $K_{a,3D}$ and $A_cK^0_{a,2D}$ as the only freely adjustable fitting parameters. This seemed reasonable, as the cell adhesion in both cases was mediated by the same CD16a/RbIgG interaction despite the fact that different soluble competitors were used. Again, good agreement was found between the model prediction and the experiment data. The best-fit values of the 3D affinity of CLBFcgran-1 Fab to CD16a and the 2D affinity of CD16a for RbIgG are listed in Table 1.

DISCUSSION

Validity of the model

The 2D/3D competition experiment is widely used for assaying the potency of a soluble inhibitor. While the data shown in Figs. 6 and 9 are commonly seen, the present work contributes a mathematical model that predicts the expected qualitative dependency of adhesion on physiochemical vari-

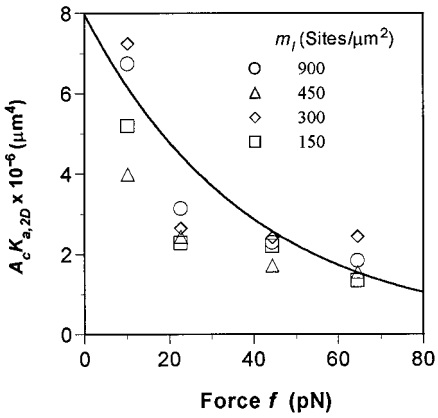

FIGURE 8 Relationship between 2D binding affinity and force on a cell. The average ratio of binding fraction, P_a (with values not exceeding 0.2), to the product of ligand density, m_l, and effective receptor density, $m_r/(1 + cK_{a,3D})$, for the points of the constant m_l curves (values indicated) shown in Fig. 6 is plotted against the force on a cell (calculated from the centrifugal speed). This provides a direct measure of $A_cK_{a,2D}(f)$, as it can be approximated by $P_a(1 + cK_{a,3D})/m_rm_l$ when P_a is small (cf. Eq. 8). The curve is a theoretical prediction based on Eq. 3 and parameter values $A_cK^0_{a,2D} = 8.0 \times 10^{-6}$ μm⁴ and $a = 0.1$ nm.

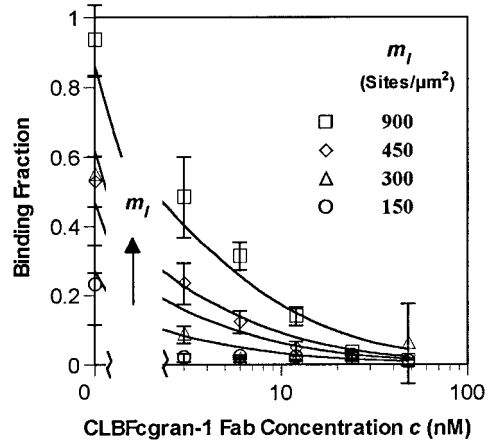

FIGURE 9 Centrifugation experiment with dissimilar competitor. Binding of CHO cells expressing 360 sites/μm² of CD16a to variable densities (indicated) of surface-bound anti-BSA RbIgG in the presence of different concentrations (0, 0.15, 0.3, 0.6, 1.2, and 2.4 ng/ml) of Fab fragment of anti-CD16 mAb CLBFcgran-1 was assayed by centrifugation (300 rpm). Data (*points*) are presented as mean ± standard deviation of quadruplicate wells. The curves are a single least χ^2 fit to all of the data based on Eqs. 2a and 3, with the best-fit parameter values shown in Table 1. The experiment was repeated three times, and the results shown are representative.

ables in a highly quantitative fashion. Moreover, comparing the theory with experiment allows us to evaluate intrinsic binding properties, such as $A_cK^0_{a,2D}$ and $K_{a,3D}$. The validity of the model has been supported by its abilities to account for the data and to predict accurately the binding properties.

To test the model rigorously, we quantified the dependence of adhesion on multiple variables over a wide range. For the similar competitor experiment (Fig. 6), the test was quite challenging: it required that the model simultaneously fit 96 data points in 16 experimental curves due to changes in three variables (c, m_l, and f). The ability of the model to account for all data using only three parameters ($K_{a,3D}$, $A_cK^0_{a,2D}$, and a) thus provided substantial support for its validity.

The fitting of the theory to the dissimilar competitor experiment (Fig. 9) was also very successful, providing further support to the model. While the competitor was changed to a mAb (CLBFcgran-1) with an affinity two to three orders of magnitude higher, it was the same 2D interaction, the binding of CD16a-expressing CHO cells to RbIgG-coated wells, that was inhibited. As such, the same 2D binding parameter should be obtained. The value of $A_cK^0_{a,2D}$ (8.0×10^{-6} μm^4) estimated from fitting the data in Fig. 6 is indeed in excellent agreement with the value (7.5×10^{-6} μm^4) calculated from the data in Fig. 9.

The same parameter has also been measured recently by a newly developed micropipette method (S. E. Chesla, P. Li, S. Nagarajan, P. Selvaraj, and C. Zhu, manuscripts submitted for publication). These workers used the same CD16a-expressing CHO cells, but the RbIgG was coated on the surface of human red blood cells. The contact area there was probably somewhat different from the A_c in the centrifugation experiment. Despite the differences in the methods and, probably, in the A_c values, the $A_cK^0_{a,2D}$ (2.8×10^{-6} μm^4) value reported by these authors is remarkably similar to those obtained herein. Thus the 2D affinity value is independent of the soluble competitors and experimental techniques used for its measurement. This indicates that it represents an intrinsic binding property of the interaction in question rather than merely a curve-fitting parameter.

Another binding property, also evaluated from comparing the predicted with the measured 2D/3D competition curves, is $K_{a,3D}$ of the cell surface CD16a for the soluble competitor. We calculated a $K_{a,3D}$ of 2.0×10^6 M^{-1} for RbIgG and 9.1×10^8 M^{-1} for CLBFcgarn-1 Fab, respectively, from the data shown in Figs. 6 and 9. These affinities were also measured using, respectively, 3D/3D competition and Scatchard analysis (S. E. Chesla, P. Li, S. Nagarajan, P. Selvaraj, and C. Zhu, manuscript submitted for publication). The values reported by these authors are 0.93×10^6 M^{-1} and 1.0×10^8 M^{-1} for RbIgG and CLBFcgarn-1 Fab, respectively. The $K_{a,3D}$ for the CD16a/RbIgG interaction is reasonably consistent with the value obtained herein. We suspect that the low $K_{a,3D}$ for CD16a/CLBFcgarn-1 interaction from our previous work might be due to iodination of CLBFcgarn-1, which might have adversely affected its binding capacity. In fact, our most recent measurement using the surface plasmon resonance technique yielded a value of 4.2×10^8 M^{-1} for CLBFcgarn-1 Fab binding to soluble CD16a (Li, 1999), which is in fair agreement with the value obtained herein.

Application to P-selectin system

Applying our model, we analyzed a 2D/3D competition binding experiment reported by Ushiyama et al. (1993). These authors coated the membrane form of P-selectin on wells of 96-well plates. The adhesion of P-selectin glycoprotein ligand 1 (PSGL-1)-expressing HL-60 cells to the coated wells was assayed by a plate inversion experiment (1-g sedimentation) in the presence of two forms of soluble monomeric P-selectin at varying concentrations. They also conducted an independent experiment of cell adhesion in the absence of soluble competitors. This allowed Piper et al. (1998) to evaluate the 2D affinity of membrane P-selectin for PSGL-1. Using this $A_cK^0_{a,2D}$ (1.3×10^{-3} μm^4) as input, we fitted the solution of Eqs. 2b and 3 to the competition data of Ushiyama et al. (1993). It is evident from Fig. 10 that the theory compares quite well with the experiment. The only curve-fitting parameter is the affinity of the soluble P-selectin. The best-fit $K_{a,3D}$ are 2.0×10^6 M and 1.8×10^6 M^{-1}, respectively, for the truncated and alternatively spliced forms of P-selectin. These values are in good agreement with the soluble P-selectin/PSGL-1 affinity ($= 3.3 \times 10^6$ M^{-1}) recently measured with the surface plasmon resonance method (Mehta et al., 1998).

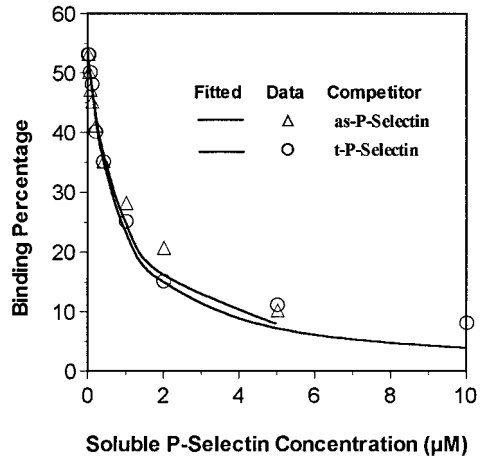

FIGURE 10 Comparison of model prediction with P-selectin data from Ushiyama et al. (1993). Adhesion of HL-60 cells (expressing 63 sites/μm^2 PSGL-1 sites for P-selectin binding) to wells of a 96-well plate coated with 10 sites/μm^2 membrane P-selectin in the presence of various concentrations of either the alternatively spliced (as-) or truncated (t-) soluble form of P-selectin was measured in a plate inversion (1-g sedimentation) assay. The curves are least χ^2 fits to the data (from Ushiyama et al., 1993, by permission), based on Eqs. 2b and 3 with predetermined parameters $A_cK^0_{a,2D} = 1.3 \times 10^{-3}$ μm^4 (Piper et al., 1998) and $a = 0.04$ nm (Alon et al., 1997). The only freely adjustable parameter is $K_{a,3D}$, the best-fit values of which are 1.8 and 2.0×10^6 M^{-1} for as- and t-P-selectin, respectively.

Relationship between IC_{50} and $K_{d,3D}$

Binding affinity reflects the propensity of the ligand to bind the receptor. IC_{50} is a measure for the potency of the soluble molecule to competitively inhibit 2D binding. The correlation between IC_{50} and $K_{d,3D}$ has been noted for quite some time (Casasnovas and Springer, 1995). The present work has derived a theoretical relationship between the two (e.g., Eq. 9), which has been tested by experiment (Fig. 7). The qualitative trends shown in Fig. 7 also make good sense intuitively. $K_{d,3D}$ can be interpreted as the concentration required for a binding curve to achieve half-saturation. For a low level of initial adhesion, due to high dislodging force or to low density of the receptor or ligand, many of the adherent cells must be mediated by just a single bond (Piper et al., 1998; Chesla et al., 1998). A concentration of the soluble competitor that would block half of the receptors would reduce half of the bonds, thereby reducing the number of adherent cells by a half. Thus $IC_{50} \approx K_{d,3D}$ when $P_a \ll 1$. If the initial level of adhesion is high, on the other hand, binding is more likely to be mediated by multiple bonds. Reducing the number of bonds by a half will weaken many adherent contacts, but less than half of them would dissociate. In other words, to reduce adhesion by a half requires a higher competitor concentration. Thus $IC_{50} > K_{d,3D}$ when $P_a \approx 1$.

Is the constant contact area assumption valid?

The contact area A_c between the adherent cell and the ligand-coated surface has been assumed constant in our model. This assumption seems reasonable during attachment because of the low number of bonds. Intuitively, A_c will not depend on the number of bonds if there exist only a few of them per cell, because bonds are only formed in a small fraction of the total contact area. In other words, when there is still a large fraction of the contact area without any bonds due to the low affinity of the CD16/IgG interaction, A_c will not increase with the increasing number of bonds until the bonds have populated all available contact area.

The evidence supporting the constant contact area assumption during detachment is as follows. Should A_c increase with the number of 2D bonds, then the parameter $A_c K^0_{a,2D}$ evaluated from curve-fitting of the centrifugation data would have been an increasing function of the binding fraction P_a instead of a constant, because the higher the P_a, the more 2D bonds there are, and the larger is A_c. This was not observed, however. To the contrary, the $A_c K^0_{a,2D}$ value calculated from fitting the entire data set of the similar competitor experiment that includes many high binding fraction data points (Fig. 6) agrees quite well with that computed using only a subset of the data that correspond to $P_a < 0.2$ (Fig. 8) and with that derived from fitting the dissimilar competitor experiment, the binding fractions of which are much lower (Fig. 9).

However, the constant contact area assumption seems counterintuitive, as we could think of an argument against it. For a cell initially bound by a few bonds, dissociation of some of them would result in readjusting the cell's position by the applied force, leading to a reduction in A_c. This issue is related to an unresolved puzzle of the centrifugation method, namely, the steady-state paradox (Piper et al., 1998).

Unresolved steady-state paradox

The reverse rates of the CD16/IgG interactions have been measured to be fractions of a reciprocal second (Chesla et al., 1998; S. E. Chesla, P. Li, S. Nagarajan, P. Selvaraj, and C. Zhu, manuscripts submitted for publication). Our model assumes that the adhesion is mediated by a low number of bonds. The question is, how could a cell bound by a few bonds of short lifetime sustain a steadily applied force? Should the contact area be reduced by the dissociation of some of the bonds, this would reduce the opportunity for rebinding, which would move the system away from the steady state toward detachment.

The achievement of steady state during the attachment phase was ensured by a long incubation time (90 min total). During the detachment phase this was verified by the lack of dependence of adhesion on the duration of force application up to 16 min (Fig. 5).

The low bond number assumption was examined very carefully. Perhaps the most compelling evidence supporting this assumption is the weakness of adhesion seen in our experiment. When the adherent fraction is small, one measure of the physical strength of cell adhesion, defined as the force required to detach 50% of the cells adherent in the absence of force, can be expressed as

$$f_{50} \approx \frac{k_B T}{a} \ln 2 \tag{11}$$

using Eqs. 3 and 8. For $a = 0.1$ nm (Table 1), $f_{50} \approx 28$ pN at room temperature. This is smaller than twice the value of the single bond strength (18 pN), determined from analyzing the histogram of over a 1000 single-cell detachment forces measured by micropipette experiment, using CD16a-expressing CHO cells and IgG-coated red cells (Zhu and Chesla, 1997). In addition, all lines of reasoning presented in our earlier publication (Piper et al., 1998) in support of the small bond number assumption also apply here.

Thus, both steady-state and small bond number assumptions seem to be supported experimentally, and we are facing the same paradox as Piper et al. (1998). In fact, one of the objectives of the present work was to reexamine this paradox by using another biological system and by extending our previous model to include soluble competitors. Unfortunately, to date we have not found an answer to this puzzle, and additional work is required to resolve the steady-state paradox.

Analysis of physiological cases

Applying the model developed herein, let us evaluate quantitatively some in vivo situations to see whether the presence of soluble receptors or ligands can inhibit 2D binding. Soluble human (h) IgG as high as 8–12 mg/ml (50–80 μM) exists in human blood (Allansmith et al., 1968). How would such a high concentration of soluble competitors influence the ability of leukocyte FcγRs to adhere to antibody-coated surfaces? Using an $A_c K^0_{a,2D}$ value of 7.4×10^{-7} μm^4 for CD16a/hIgG interaction (Chesla et al., 1998) and assuming m_r and m_l to be 100 and 1000 sites/μm^2 respectively, Eq. 8 predicts an adhesion probability of 7.4% in the absence of a soluble competitor without force. Taking a $K_{a,3D}$ value of 2.5×10^5 M^{-1} for the same CD16a/hIgG interaction (S. E. Chesla, P. Li, S. Nagarajan, P. Selvaraj, and C. Zhu, manuscript submitted for publication), Eq. 10a predicts ~95% inhibition by the presence of 80 μM serum IgG. Similar predictions can be made for other FcγRs if they also have a similar $K_{a,3D}/K^0_{a,2D}$ ratio. This suggests that without other priming mechanisms to either decrease the $K_{a,3D}/K^0_{a,2D}$ ratio or increase m_r, FcγR-mediated leukocyte adhesion to targets (e.g., opsonized bacteria or immune complex deposited on vessel walls) would be a rare occurrence, even for m_l as high as 1000 sites/μm^2.

Soluble P-selectin is present in human plasma at a concentration of 30–300 ng/ml (0.2–2 nM) in healthy subjects and severalfold higher in patients with thrombotic disorders (Dunlop et al., 1992; Katayama et al., 1993; Ushiyama et al., 1993; Chong et al., 1994). These are at least two orders of magnitude lower than the $K_{d,3D}$ (300–550 nM) for PSGL-1, the only high-affinity ligand on leukocytes for P-selectin. Such low circulating concentrations would not be able to competitively inhibit the PSGL-1-mediated binding of leukocytes to P-selectin-expressing cells such as platelets and vascular endothelial cells. It should be emphasized that this prediction does not exclude other possible regulatory roles of soluble P-selectin. Similarly, while soluble CD16 exists in circulation, the concentration (2.7 μg/ml; Mathiot et al., 1993) is ~30 times lower than its $K_{d,3D}$ for hIgG. If soluble CD16 could only serve an adhesion antagonist role, our model predicts a minimal effect for it in blocking CD16/hIgG-mediated adhesion. These examples illustrate the usefulness of Eqs. 7–10 in analyzing situations that involve 2D/3D competition binding.

We thank Dr. S. Nagarajan for technical assistance in gel filtration and fluoremetric measurement and Dr. M. Long for assistance in numerical computations. We also thank Dr. R. P. McEver for allowing us to use the previously published data (Fig. 10) and for suggesting that we analyze the soluble P-selectin case.

This work was supported by National Science Foundation grant BCS 9350370 and National Institutes of Health grant AI38282.

REFERENCES

Allansmith, M., B. H. McClellan, M. Butterworth, and J. R. Maloney. 1968. The development of immunoglobulin levels in man. *J. Pediatr.* 72:276–290.

Alon, R., S. Chen, K. D. Puri, E. B. Finger, and T. A. Springer. 1997. The kinetics of L-selectin tethers and the mechanics of selectin-mediated rolling. *J. Cell Biol.* 138:1169–1180.

Bikoue, A., F. George, P. Poncelet, M. Mutin, G. Janossy, and J. Sampol. 1996. Quantitative analysis of leukocyte membrane antigen expression: normal adult values. *Cytometry.* 26:137–147.

Capon, D. J., S. M. Chamow, J. Mordenti, S. A. Marsters, T. Gregory, H. Mitsuya, R. A. Byrn, C. Lucas, F. M. Wurm, J. E. Groopman, S. Broder, and D. H. Smith. 1989. Designing CD4 immunoadhesins for AIDS therapy. *Nature.* 337:525–531.

Casasnovas, J. M., and T. A. Springer. 1995. Kinetics and thermodynamics of virus binding to receptor. Studies with rhinovirus, intercellular adhesion molecule-1 (ICAM-1), and surface plasmon resonance. *J. Biol. Chem.* 270:13216–13224.

Cheng, Y., and W. H. Prusoff. 1973. Relationship between the inhibition constant (K1) and the concentration of inhibitor which causes 50 per cent inhibition (I50) of an enzymatic reaction. *Biochem. Pharmacol.* 22:3099–3108.

Chesla, S. E., P. Selvaraj, and C. Zhu. 1998. Measuring two-dimensional receptor-ligand binding kinetics by micropipette. *Biophys. J.* 75: 1553–1572.

Chong, B. H., B. Murray, M. C. Berndt, L. C. Dunlop, T. Brighton, and C. N. Chesterman. 1994. Plasma P-selectin is increased in thrombotic consumptive platelet disorders. *Blood.* 83:1535–1541.

Chorev, M., R. Dresner-Pollak, Y. Eshel, and M. Rosenblatt. 1995. Approach to discovering novel therapeutic agents for osteoporosis based on integrin receptor blockade. *Biopolymers.* 37:367–375.

Clarkson, S. B., J. B. Bussel, R. P. Kimberly, J. E. Valinsky, R. L. Nachman, and J. C. Unkeless. 1986. Treatment of refractory immune thrombocytopenic purpura with an anti-Fc gamma-receptor antibody. *N. Engl. J. Med.* 314:1236–1239.

Crandall, I., W. E. Collins, J. Gysin, and I. W. Sherman. 1993. Synthetic peptides based on motifs present in human band 3 protein inhibit cytoadherence/sequestration of the malaria parasite *Plasmodium falciparum. Proc. Natl. Acad. Sci. USA.* 90:4703–4707.

Dresner-Pollak, R., and M. Rosenblatt. 1994. Blockade of osteoclast-mediated bone resorption through occupancy of the integrin receptor: a potential approach to the therapy of osteoporosis. *J. Cell. Biochem.* 56:323–330.

Dunlop, L. C., M. P. Skinner, L. J. Bendall, E. J. Favaloro, P. A. Castaldi, J. J. Gorman, J. R. Gamble, M. A. Vadas, and M. C. Berndt. 1992. Characterization of GMP-140 (P-selectin) as a circulating plasma protein. *J. Exp. Med.* 175:1147–1150.

Edberg, J. C., and R. P. Kimberly. 1997. Cell type-specific glycoforms of Fc gamma RIIIa (CD16): differential ligand binding. *J. Immunol.* 159: 3849–3857.

Heaney, M. L., and D. W. Golde. 1998. Soluble receptors in human disease. *J. Leukoc. Biol.* 64:135–146.

Hibbs, M. L., P. Selvaraj, O. Carpen, T. A. Springer, H. Kuster, M. H. Jouvin, and J. P. Kinet. 1989. Mechanisms for regulating expression of membrane isoforms of Fc gamma RIII (CD16). *Science.* 246: 1608–1611.

Jameson, S. C., and M. J. Bevan. 1995. T cell receptor antagonists and partial agonists. *Immunity.* 2:1–11.

Kalinke, U., A. Krebber, C. Krebber, E. Bucher, A. Pluckthun, R. M. Zinkernagel, and H. Hengartner. 1996. Monovalent single-chain Fv fragments and bivalent miniantibodies bound to vesicular stomatitis virus protect against lethal infection. *Eur. J. Immunol.* 26:2801–2806.

Katayama, M., M. Handa, Y. Araki, H. Ambo, Y. Kawai, K. Watanabe, and Y. Ikeda. 1993. Soluble P-selectin is present in normal circulation and its plasma level is elevated in patients with thrombotic thrombocytopenic purpura and haemolytic uraemic syndrome. *Br. J. Haematol.* 84:702–710.

Kotze, H. F., P. N. Badenhorst, S. Lamprecht, M. Meiring, V. Van Wyk, K. Nuyts, J. M. Stassen, J. Vermylen, and H. Deckmyn. 1995. Prolonged inhibition of acute arterial thrombosis by high dosing of a monoclonal anti-platelet glycoprotein IIb/IIIa antibody in a baboon model. *Thromb. Haemost.* 74:751–757.

Lanier, L. L., G. Yu, and J. H. Phillips. 1989. Co-association of CD3 zeta with a receptor (CD16) for IgG Fc on human natural killer cells. *Nature.* 342:803–805.

Letourneur, O., I. C. Kennedy, A. T. Brini, J. R. Ortaldo, J. J. O'Shea, and J. P. Kinet. 1991. Characterization of the family of dimers associated with Fc receptors (Fc epsilon RI and Fc gamma RIII). *J. Immunol.* 147:2652–2656.

Li, P. 1999. The characteristics of CD16a binding and its inhibition. Ph.D. thesis. Georgia Institute of Technology.

Long, M., G. L. Goldsmith, D. F. J. Tees, and C. Zhu. 1999. Probabilistic modeling of shear-induced formation and breakage of doublets cross-linked by receptor-ligand bonds. *Biophys. J.* 76:1112–1128.

Martin, S., J. M. Casasnovas, D. E. Staunton, and T. A. Springer. 1993. Efficient neutralization and disruption of rhinovirus by chimeric ICAM-1/immunoglobulin molecules. *J. Virol.* 67:3561–3568.

Mathiot, C., J. L. Teillaud, M. Elmalek, V. Mosseri, L. Euller-Ziegler, A. Daragon, B. Grosbois, J. L. Michaux, T. Facon, J.-F. Bernard, B. Duclus, M. Moncondutt, and W. H. Fridman. 1993. Correlation between soluble serum CD16 (sCD16) levels and disease stage in patients with multiple myeloma. *J. Clin. Immunol.* 13:41–48.

McClay, D. R., G. M. Wessel, and R. B. Marchase. 1981. Intercellular recognition: quantitation of initial binding events. *Proc. Natl. Acad. Sci. USA.* 78:4975–4979.

McQuarrie, D. A. 1963. Kinetics of small systems. I. *J. Chem. Phys.* 38:433–436.

Mehta, P., R. D. Cummings, and R. P. McEver. 1998. Affinity and kinetic analysis of P-selectin binding to P-selectin glycoprotein ligand-1. *J. Biol. Chem.* 273:32506–32513.

Nagarajan, S., S. Chesla, L. Cobern, P. Anderson, C. Zhu, and P. Selvaraj. 1995. Ligand binding and phagocytosis by CD16 (Fc gamma receptor III) isoforms. Phagocytic signaling by associated zeta and gamma subunits in Chinese hamster ovary cells. *J. Biol. Chem.* 270:25762–25770.

O'Shea, J. J., A. M. Weissman, I. C. Kennedy, and J. R. Ortaldo. 1991. Engagement of the natural killer cell IgG Fc receptor results in tyrosine phosphorylation of the zeta chain. *Proc. Natl. Acad. Sci. USA.* 88: 350–354.

Piper, J. W., R. A. Swerlick, and C. Zhu. 1998. Determining force dependence of two-dimensional receptor-ligand binding affinity by centrifugation. *Biophys. J.* 74:492–513.

Scallon, B. J., E. Scigliano, V. H. Freedman, M. C. Miedel, Y. C. Pan, J. C. Unkeless, and J. P. Kochan. 1989. A human immunoglobulin G receptor exists in both polypeptide-anchored and phosphatidylinositol-glycan-anchored forms. *Proc. Natl. Acad. Sci. USA.* 86:5079–5083.

Scatchard, G. 1949. The attraction of proteins for small molecules and ions. *Ann. N.Y. Acad. Sci.* 51:660–672.

Selvaraj, P., O. Carpen, M. L. Hibbs, and T. A. Springer. 1989. Natural killer cell and granulocyte Fc gamma receptor III (CD16) differ in membrane anchor and signal transduction. *J. Immunol.* 143:3283–3288.

Selvaraj, P., W. F. Rosse, R. Silber, and T. A. Springer. 1988. The major Fc receptor in blood has a phosphatidylinositol anchor and is deficient in paroxysmal nocturnal haemoglobinuria. *Nature.* 333:565–567.

Serke, S., A. van Lessen, and D. Huhn. 1998. Quantitative fluorescence flow cytometry: a comparison of the three techniques for direct and indirect immunofluorescence. *Cytometry.* 33:179–187.

Ushiyama, S., T. M. Laue, K. L. Moore, H. P. Erickson, and R. P. McEver. 1993. Structural and functional characterization of monomeric soluble P-selectin and comparison with membrane P-selectin. *J. Biol. Chem.* 268:15229–15237.

Wallace, P. K., T. Keler, P. M. Guyre, and M. W. Fanger. 1997. Fc gamma RI blockade and modulation for immunotherapy. *Cancer Immunol. Immunother.* 45:137–141.

Williams, T. E. 1998. Adhesion of membrane-bound receptors and ligands: concurrent binding and the role of microtopology. Ph.D. thesis. Georgia Institute of Technology.

Zhu, C., and S. E. Chesla. 1997. Dissociation of individual molecular bonds under force. *In* 1997 Advances in Bioengineering, BED, Vol. 36. B. Simon, editor. New York, ASME. 177–178.

Zhu, C., J. W. Piper, and R. A. Swerlick. 1999. A centrifugation method for measurement of two-dimensional binding characteristics of receptor-ligand interaction. *In* Bioadhesion in Drug Delivery: Issues in Fundamentals, Novel Approaches, and Development. E. Mathiowitz, D. E. Chickering III, and C.-M. Lehr, editors. Marcel Dekker, New York. 261–298.